Evaluation of Skeletal and Soft Tissue Contributions to Thoracic Response of GHBMC M50-O Model in Dynamic Frontal Loading Scenarios

R. Ramachandra, YS. Kang, J. Stammen, K. Moorhouse, M. Murach, J. Bolte IV, A. Agnew

Abstract This study investigated the response of the Global Human Body Models Consortium (GHBMC) M50-O v4.5 model in a simulated thoracic impact and compared to the responses of post-mortem human subjects (PMHS) in physical experiments. The model was simulated in four tissue states: intact, intact with upper limbs removed, denuded (superficial tissue removed), and eviscerated (superficial tissue and viscera removed). The GHBMC model was subjected to a 3 m/s frontal thoracic impact using a 23 kg impactor, with the model seated upright in a fixed-back configuration. Force-compression results from the simulations were compared directly to PMHS responses from the series of frontal impacts limited to ≤20% chest compression. Biofidelity of the GHBMC thorax responses were quantified using the NHTSA Biofidelity Ranking System (BioRank). Additionally, individual mid-level ribs from the GHBMC were extracted and simulated in the isolated rib bending test scenario. The force-displacement and fracture location were compared to the physical experiments on the same ribs. In the thoracic loading simulations, the GHBMC exhibited biofidelity scores of 1.6, 1.5, 2.4 and 1.6 in the intact, upper limbs removed, denuded and eviscerated conditions, respectively. The scores were deemed acceptable (BioRank<2.0) in three of four conditions. The individual rib simulations resulted in a peak force of approximately 150N at fracture. This fracture occurred when the effective plastic strain reached 1.8% and at a location closer to the vertebral end than the experiment. The force-displacement responses of the GHBMC ribs were similar to the experimental tests of the corresponding ribs.

Keywords GHBMC, thorax, impactor, rib

I. INTRODUCTION

Finite element (FE) human body models (HBM) are becoming more frequently utilized to assess biomechanical response and potentially injury risk, but finding the correct injury tolerance or developing a risk function for such models requires a detailed mapping of human variation and response data from post mortem human subject (PMHS) tests. Most material properties for hard and soft tissue used in models are characterized using isolated component tests and assumed to also be valid for whole body simulations. While such full body assessments are important to assess the injury prediction capability of FE HBMs, the exact contributions of different structures are not often compared against experimental data. The human thorax is one such body region that is complicated to model, given its geometric and material heterogeneity (bony ribcage, viscera, musculature and skin), as well as the contribution of these soft and hard tissues to the overall biomechanical response. Given that thoracic injuries are a leading cause of death in motor vehicle crashes (MVCs) [1-4] and rib fractures are the most common thoracic injuries, it is important to understand the distinction and contributions of tissue types to thoracic response.

FE models of the human thorax have been developed with great detail in HBMs to investigate the structural response of the thorax in efforts to establish injury tolerance [5-8]. One such detailed HBM was created by the Global Human Body Model Consortium (GHBMC) to represent a 50th percentile male (M50-O) in a standard vehicle occupant seated posture. The GHBMC M50-O is comprised of 2.2 million elements and 1.3 million nodes representing detailed anatomical geometry based on medical imaging of a 26 year-old male [9]. The biofidelity of the GHBMC thorax has been evaluated using pendulum impacts (frontal and oblique at 4.3 m/s, lateral at 2.5 m/s)[9]. The model has also been evaluated against distributed loading scenarios, and more recently, a point loading evaluation was performed on the eviscerated ribcage of the GHBMC [10-11].

R. Ramachandra (ramachandra.6@osu.edu / +1 614 366 7767), YS. Kang, JH. Bolte IV and A. Agnew are PhDs at the Injury Biomechanics Research Center at The Ohio State University, Columbus, OH, USA. J. Stammen and K. Moorhouse are PhDs at National Highway Traffic Safety Administration, Vehicle Research & Test Center, U.S. Department of Transportation, Washington, DC, USA. M. Murach is an Engineer at Transportation Research Center Inc., East Liberty, OH, USA.

In all the evaluation scenarios, the overall impact force and compression responses of the thorax were used as criteria to assess the GHBMC model. While this is a reasonable approach for comparing PMHS response to anthropometric test devices (ATDs), it does not fully characterize the injury outcome of a human thorax. One of the advantages of using FE models instead of ATDs is the potential to provide more detailed information about injury mechanisms. Hence, additional validation of the thorax at sub-structural levels in a hierarchical manner would provide more accurate global model responses and minimize adjustments to material properties in order to match experimental data. However, few experimental studies exist that provide any insight of the influence of each thoracic component to the fully intact thoracic response.

Recently, a series of non-injurious frontal dynamic thoracic impacts were conducted on PMHS approximating a 50th percentile male [13]. To quantify the effect of all thoracic components, each PMHS was tested in four sequential tissue states: intact, intact without upper limbs, denuded (superficial tissue removed), and eviscerated (superficial tissue and viscera removed). The series was followed by individual rib testing to failure in a preliminary attempt to predict eviscerated thoracic response from a single rib response. This prediction was not adequate due to the unknown contributions of the sub-structural, non-rib portions of the thorax, which may be more successfully quantified by the GHBMC. Therefore, the objective of this study was to evaluate the biofidelity of the GHBMC thorax subjected to a dynamic loading scenario identical to [13] for different tissue states in order to confirm whether it is appropriate to use the model to help quantify the contributions of superficial tissue, viscera, and the rib cage to thoracic response when subjected to anterior hub loading. The extended objective is to use the simulation work in tandem with the results of thoracic hierarchy PMHS testing to use individual rib response data to predict overall thoracic response, that may be extended to HBM or ATDs of demographics for which there is limited full-body response data, but for which individual rib data can be obtained.

II. METHODS

Thoracic Hierarchy Simulations

Following the methodology of the PMHS tests in [13], a fixed back scenario was utilized in order to create a whole-body loading environment analogous to that of the individual rib tests (i.e., the vertebral end is fixed translationally but free to rotate). The anthropometric data for PMHS in the physical experiments and the GHBMC are provided in Table A1. Since the default posture of the GHBMC reflects an occupant seated in a vehicle environment, it was first repositioned to assume the axes orientation of the PMHS in the actual experimental setup. Fig. 1 shows the adjusted, pre-test position of the GHBMC in the intact condition. The GHBMC was seated on a flat rigid surface which was created using the RIGIDWALL_GEOMETRIC_FLAT command. A curved rigid plate created using Belytschko-Tsay shell elements was utilized to arrest any spinal motion posteriorly. The anterior thorax was impacted using a 23 kg impactor with a 6” high x 12” wide rectangular face centered vertically and horizontally on the sternum, similar to the PMHS study. The impactor was modeled using fully integrated selective reduced solid elements. Rigid material (MAT_20, LS-Dyna) was assigned to both the back plate and the impactor.

Fig. 1. Pre-impact position of the GHBMC in the intact condition

To quantify the effect of all thoracic components, the GHBMC was simulated in four tissue states: intact, intact without upper limbs, denuded (superficial tissue removed), and eviscerated (superficial tissue and viscera removed) (Fig. 2). Removal of the upper limbs included disarticulation at the humeral head and disconnecting the pectoralis major and latissimus dorsi muscles from their insertion points in the bicipital groove. All parts in the upper limb were then removed past the stiff flesh in the shoulder. The denuding process involved removing all skin, flesh and fat parts from the thorax. The pectoralis major, pectoralis minor, trapezius, latissimus dorsi, rhomboid major, and rhomboid minor muscles were also removed. Lastly, for the eviscerated condition, all parts including the thoracic and abdominal organs were removed. The clavicles were left intact and attached to the thorax at the sternoclavicular joint in all tissue states. In all cases, the Constrained_Nodal_Rigid_Bodies (CNRBs) and Contact_Tied_Nodes belonging to the "dissected out" parts were identified and removed. The intercostal muscles and intrinsic back muscles were left intact in all cases. The seated chest depth in each tissue state for the GHBMC along with the PMHS are provided in Table A2.

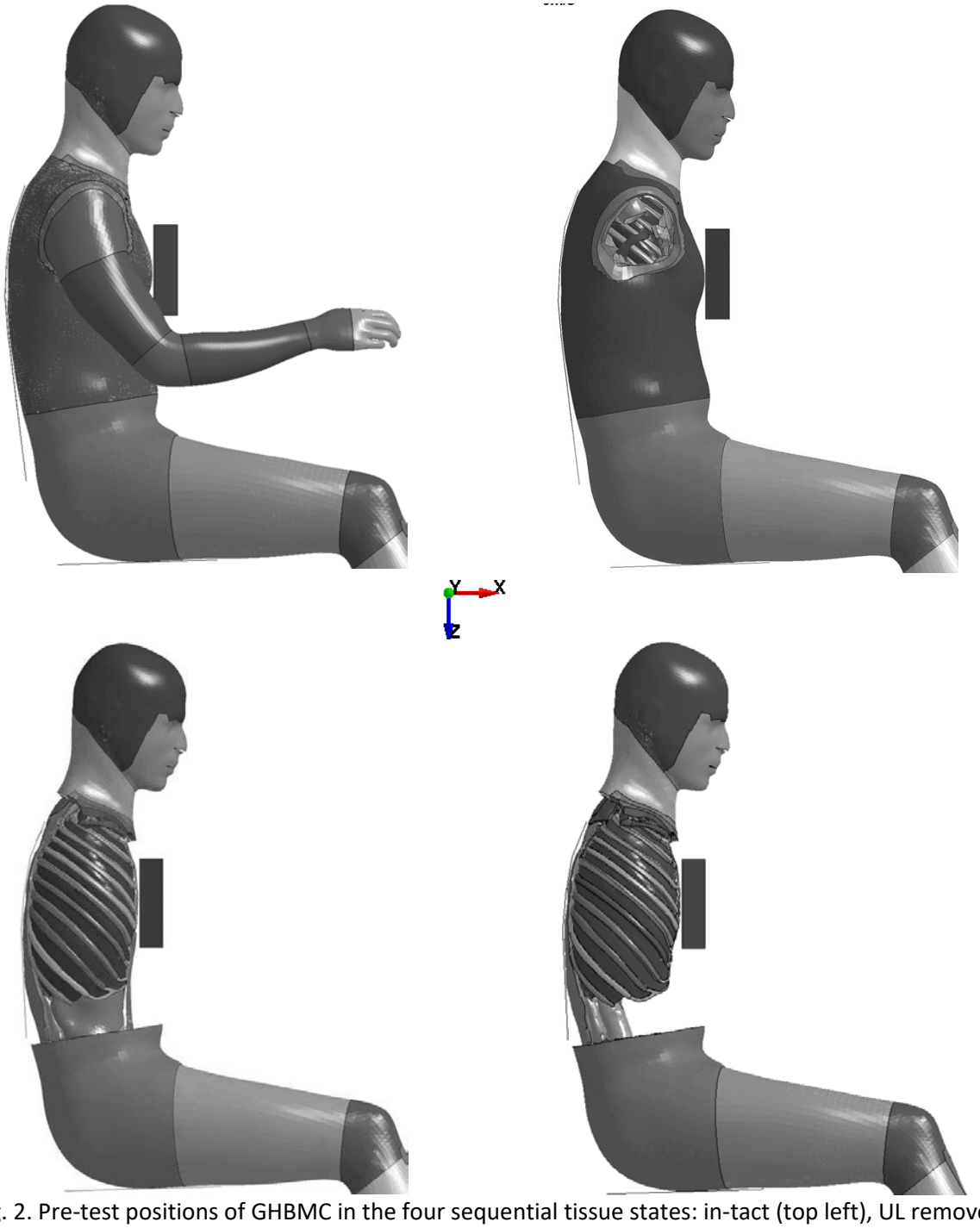

Fig. 2. Pre-test positions of GHBMC in the four sequential tissue states: in-tact (top left), UL removed (top right), denuded (bottom left), and eviscerated (bottom right).

Contact definitions were added to the model setup using the CONTACT_AUTOMATIC_SURFACE_TO _SURFACE command between the exterior skin of the GHBMC and the impactor, as well as between the skin and back plate, for the intact and upper limbs removed cases. These definitions were modified in the simulations with denuded and eviscerated GHBMC, where the skin was replaced with segment sets comprised of the ribs, sternum and intercostal muscles anteriorly, and the vertebral bodies, ribs, intercostal and back muscles posteriorly. A frictional coefficient of 0.3 was selected for the contact definitions. The impactor plate was constrained in all degrees-of-freedom (DOF) except translation in the global X direction. An initial velocity of 3 m/s was prescribed to the impactor using the INITIAL_VELOCITY_GENETRATION command at contact with the anterior aspect of the thorax at mid-sternum. Unlike in PMHS experiments, compression of the thorax was not limited since any additional response data was simply excluded from analysis. The GHBMC uses a 2.5 mm average element size and an elastic-plastic material model (MAT_24, LS-Dyna) for the cortical bone of ribs. The size of the rib elements and the rib material properties were not modified.

The simulations were run using LS-Dyna v 971 MPP 9.01 (Livermore Software Technology Corporation, Livermore, CA) using 28 processors on the Owens cluster at the Ohio Supercomputer Center. Outputs from the simulations were analyzed using LS-prepost 4.5.17 (Livermore Software Technology Corporation, Livermore, CA). Data were acquired per standard SAE-J211 [14], with the positive X directed from posterior to anterior, positive Y directed from left to right, and positive Z directed from superior to inferior. Thorax displacement was measured using the x-displacement of the impactor.

The anterior force was measured on the impactor plate using a contact-related force output, DATABASE_RCFORC, with resultant contact forces for the impactor and GHBMC. All data were truncated when 20% chest compression was reached. The force and displacement data were filtered using Channel Frequency Class (CFC) 180. Compression of the thorax was defined as the percentage of displacement, calculated by dividing the impactor displacement by initial thorax depth measured for each condition. Stiffness (k) was calculated for the linear spring model containing equal potential energy as the thorax at 20% chest compression (δ_{20}) (Equation 1) consistent with the PMHS data processing and analysis [13].

$$PE = \frac{1}{2}k{\delta_{20}}^2 \rightarrow k = \frac{2PE}{{\delta_{20}}^2}, where\ PE = \int_0^{\delta_{20}} F \cdot d\delta \quad (1)$$

In order to quantitatively assess the similarity of the GHBMC responses to the PMHS-based corridors, an objective biofidelity ranking score was calculated using the methodology described by Rhule et al. [15]. The force channels were first brought to a common compression basis across the PMHS tests and GHBMC simulations. Equation 2 shows the calculation used for generating a biofidelity score. The √R value corresponds to the ratio of cumulative variance between the GHBMC response and mean PMHS response over the cumulative variance between the mean PMHS response and mean plus one standard deviation. A lower value of the Biofidelity Rank (BR) represents better biofidelity.

$$BR = \frac{\sum_{i=1}^{l}\left[\frac{\sum_{j=1}^{m}\left[\frac{\sum_{k=1}^{n}\sqrt{R_{i,j,k}}}{n}\right]}{m}\right]}{l} \quad (2)$$

where R = response measurement comparison value, i = body region, j = test condition, k = response measurement, l = number of body regions = 1 (thorax), m = number of test conditions = 1 (impactor loading), and n = number of response measurements per test condition = 1 (force).

Force at 20% chest compression and stiffness values from the simulations were compared to the corresponding average values from PMHS 02 – 06 from [13]. Additionally, force fraction (FF) and stiffness fraction (SF) were calculated by dividing the value from the tissue state of interest by the value calculated for the intact tissue state. These values represent the force or stiffness that each tissue condition retained when compared to the intact

condition. The closer these values are to one, the more similar the responses. These FF and SF values for the simulations were then compared to the corresponding PMHS outcomes.

Individual Rib Simulations

The right fourth and sixth ribs were isolated from the GHBMC at the costovertebral and sternocostal joints. Each rib was set up in a model simulating the boundary conditions described in [13, 16-17]. The cortical and trabecular aspects of the rib were included, and the size of the rib elements and the rib material properties were not modified. The vertebral (posterior) and sternal (anterior) rib ends were attached to a potting resin created using solid element formulation and linear elastic material properties were applied, with Young's modulus E=2.2 GPa and Poisson's ratio v=0.34 [18]. The bottom of the potting resin was attached to aluminum cups on both the vertebral and sternal ends using shared nodes. Each cup was allowed to rotate within a corresponding housing using two rotational pin joints defined by AUTOMATIC_SURFACE_TO_SURFACE contact definitions. A rigid material law (MAT_20) was assigned to both the vertebral and sternal end housings.

Two methods of loading were investigated simulating a frontal impact to the thorax in which the sternal end of the rib was linearly translated toward the vertebral end. The first method included applying a BOUNDARY_PRESCRIBED_MOTION_RIGID (BPM) to the sternal end housing in the negative X direction. A displacement-time history was used for the BPM that was derived from the individual rib experiments in [13]. In the second method, the sternal housing was impacted using a 54.4 kg impactor as in the experiment, modeled using fully integrated selective reduced solid elements. A rigid material law (MAT_20, LS-Dyna) was assigned to the impactor. An initial velocity of 2 m/s was prescribed to the impactor using INITIAL_VELOCITY_GENETRATION command at contact with the sternal housing. This method allowed the rib to be loaded until failure in case the peak displacement in the former method was insufficient to fracture the rib. In both methods, the vertebral end housing was constrained in all degrees-of-freedom (DOF), and the sternal end housing was constrained in all but translational X direction DOF.

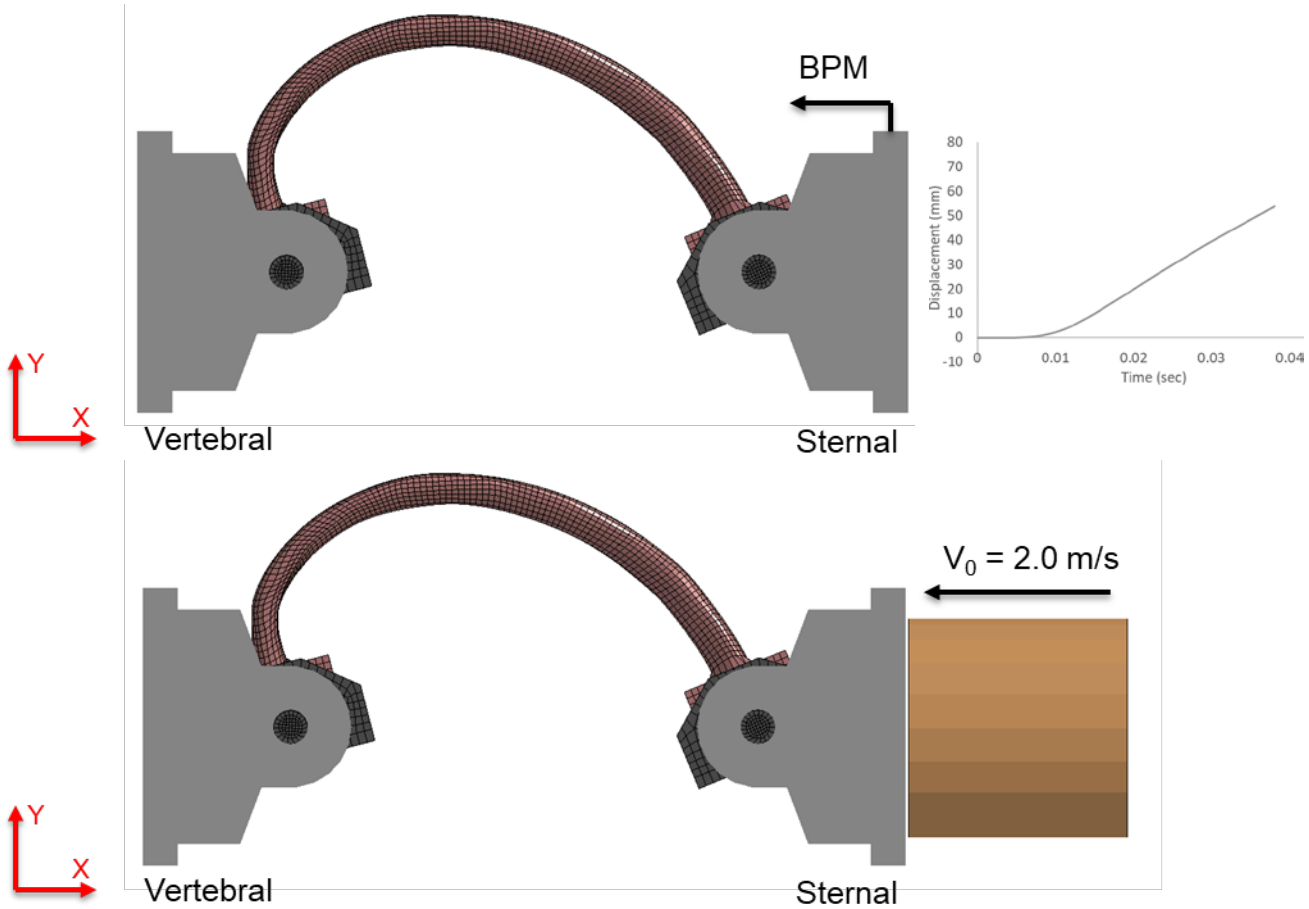

Fig. 3. Pre-test setup of GHBMC right fourth individual rib simulations. Method 1 (top) consisted of prescribed rigid body motion (BPM) using the average displacement time history from the individual rib tests applied to the sternal end housing (in light gray) in the X direction; Method 2 (bottom) consisted of a 54.4 kg impactor applied at initial velocity of 2 m/s. Similar models were developed for the right sixth rib of the GHBMC.

Like in the full thorax simulations, these individual rib simulations were run using LS-Dyna v 971 SMP 9.01 and the outputs from the simulations were analyzed using LS-prepost 4.5.17. Data were again acquired per standard SAE-J211. The reaction force was measured on the vertebral end using a contact-related force output, DATABASE_RCFORC. The force data were filtered using CFC 180 and plotted against displacement data. The force-displacement responses from the two individual level rib simulations were compared to the corresponding level rib tests from [13]. For a quantitative assessment, an objective biofidelity ranking score was calculated for the 4th and 6th ribs simulated with BPM, using a methodology similar to the full thorax simulations. Additionally, the cortical bone strains and fracture locations based on elements with maximum effective plastic strain were compared between the FE simulations and rib experiments.

III. RESULTS

Thoracic Hierarchy Simulations

The GHBMC was simulated in four tissue states: intact, intact without upper limbs, denuded (superficial tissue removed), and eviscerated (superficial tissue and viscera removed), all truncated at 20% chest compression. Snapshots of the simulations at 0, 5, 10, 15 and 20% compressions are provided in Fig. A1. The force-displacement curves, generated by plotting the anterior force data against the displacement of the impactor up to 20% chest compression from all four simulations are shown in Fig. 4. Table I catalogues the force at 20% chest compression and stiffness from GHBMC simulations and PMHS tests.

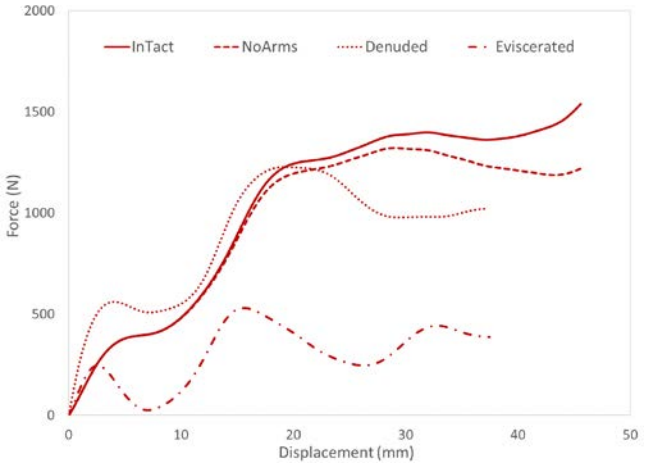

Fig. 4. Force-displacement (left) and stiffness-displacement (right) curves for GHBMC

TABLE I
SUMMARY OF FORCE AND STIFFNESS VALUES AT 20% PEAK COMPRESSION

Condition	*Force (N)*		*Stiffness (N/mm)*	
	PMHS Avg. + 1 St. Dev	*GHBMC*	*PMHS Avg. + 1 St. Dev*	*GHBMC*
Intact	1297 ± 56	1524	45.4 ± 6.6	45.1
Intact - UL	1350 ± 68	1213	42.8 ± 5.0	42.3
Denuded	1151 ± 56	1020	31.0 ± 4.9	47.2
Eviscerated	599 ± 51	387	13.0 ± 2.8	15.2

The GHBMC force and compression response compared to the average PMHS response (calculated from PMHS 02 – 06) with corridors (± one standard deviation) for each of the four tissue states are in Fig. 5. Since displacement was both linear and controlled, a common compression vector was established and force data were interpolated to create the independent variable utilized for the BioRank (BR) calculation (Table II). GHBMC with intact thorax, GHBMC with intact thorax but upper limbs removed, and GHBMC with eviscerated thorax demonstrated overall BR under 2.0, suggesting a biofidelic response [19]. With a difference in Biofidelity Rank of under 0.2 between these three models, they are considered to be similar to each other with respect to biofidelity [15]. However, the GHBMC with denuded thorax had the highest BR indicating the least biofidelic response in this

particular test configuration.

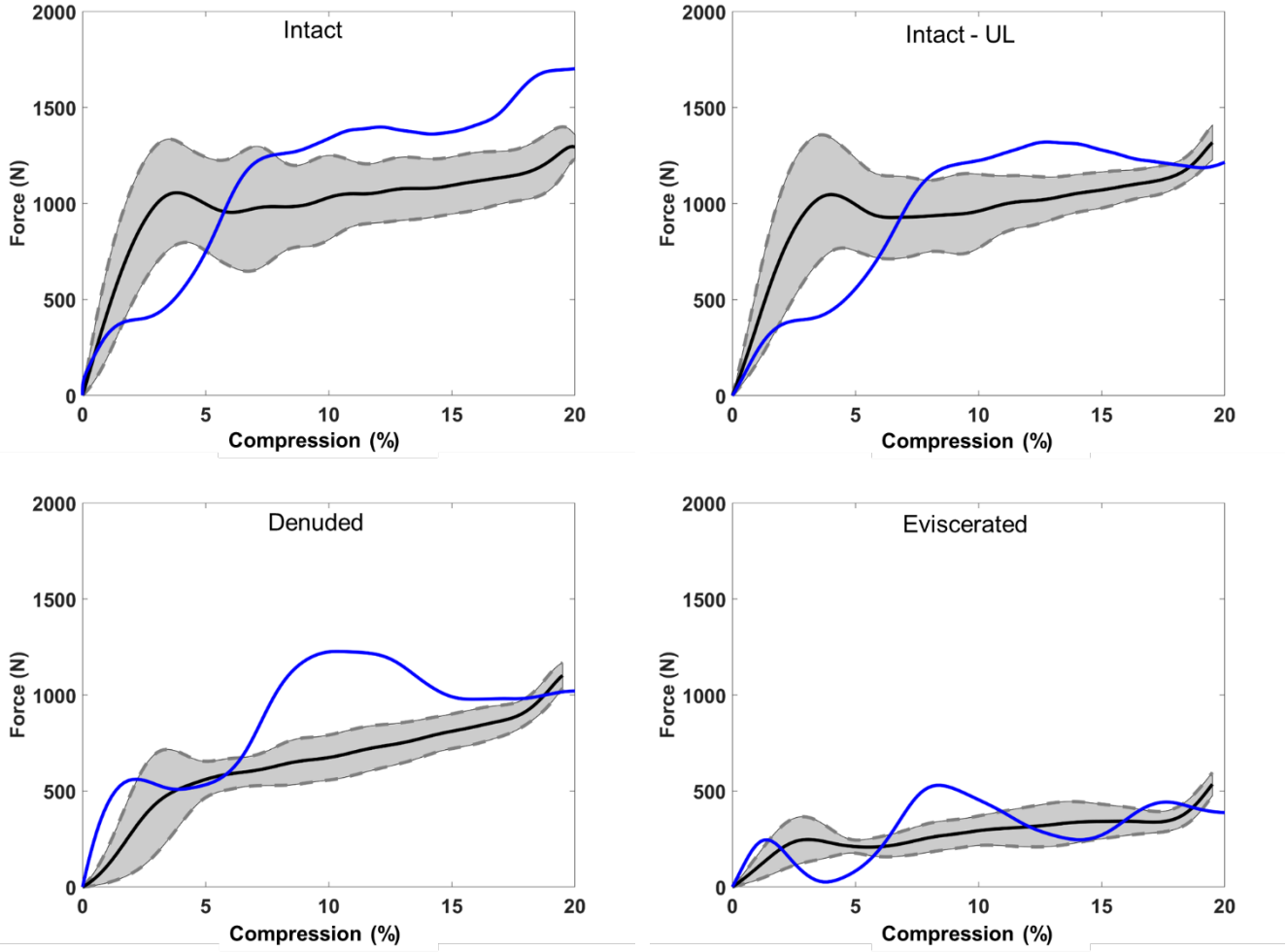

Fig. 5. Anterior force-compression corridors for PMHS 02 – 06 (black) with GHBMC (blue) force-compression curves overlaid: intact (top left), intact–UL (top right), denuded (bottom left), and eviscerated (bottom right).

TABLE II
BIOFIDELITY RANKS FOR GHBMC

Condition	*Force-Compression*
Intact	1.6
Intact - UL	1.5
Denuded	2.4
Eviscerated	1.6

Comparisons of force fractions (FF) and stiffness fractions (SF) between the GHBMC and PMHS are in Fig. 6 and Fig. 7 respectively. The model retained 79% of force and 94% of stiffness with the upper limbs removed. The SF values were similar between the GHBMC and PMHS, but the FF was considerably higher for the PMHS than for GHBMC. The denuded thorax of the GHBMC retained 67% of impact force compared to the PMHS average of 89%, while the opposite was true for stiffness with the calculated SF much higher for the GHBMC at 104% compared to 70% for the PMHS. The model retained 26% of force and 34% of stiffness when the thorax was eviscerated, and the SF values were similar between the GHBMC and PMHS.

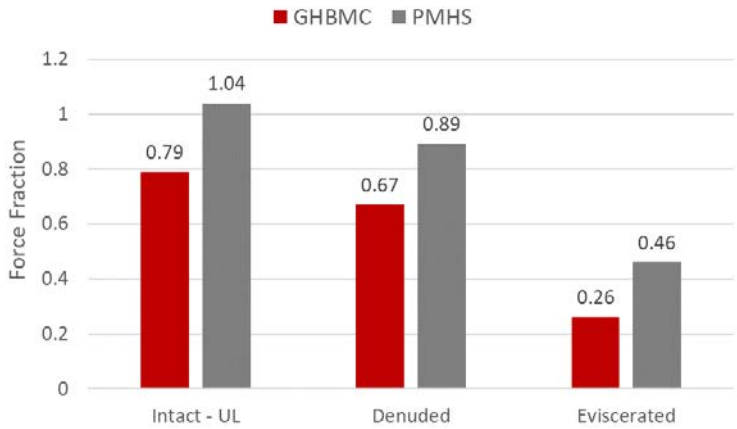

Fig. 6. Force fractions for GHBMC in comparison with PMHS at 20% chest compression.

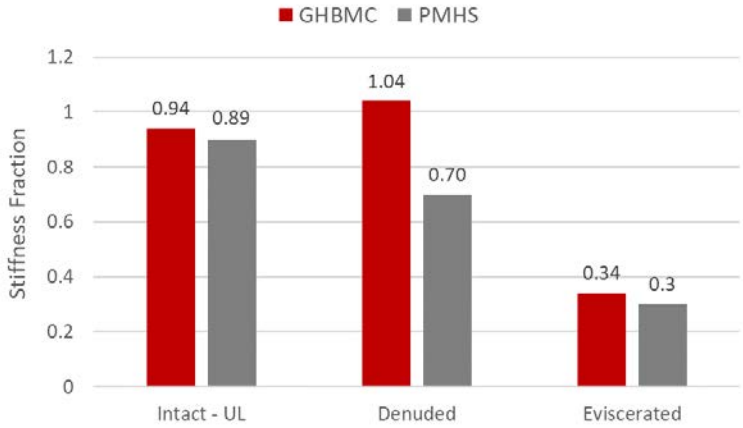

Fig. 7. Stiffness fractions for GHBMC in comparison with PMHS at 20% chest compression.

Individual Rib Simulations

The peak forces of individual ribs from GHBMC ranged from 145 to 154 N across all four simulations. Force-displacement curves of fourth and sixth individual rib simulations in comparison with the individual PMHS rib testing are in Fig. 8. There was not a considerable difference in the force-displacement response between the two methods of providing input. The simulation with the impactor allowed the sternal end of the rib to displace further than the peak displacement of the BPM, resulting in a fracture closer to the vertebral end. No distinction could be made between ribs four and six from the individual rib simulations based on the force-displacement data.

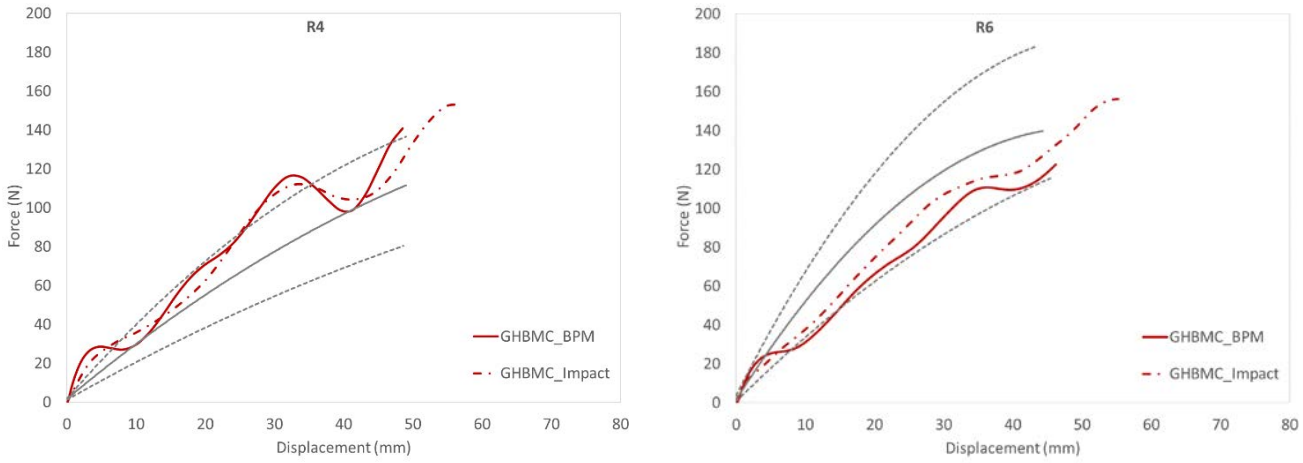

Fig. 8. Rib force-displacement corridors for PMHS (mean- solid gray; 1SD dashed gray) and individual GHBMC curves: right rib 4 (left), and right rib 6 (right)

Since displacement was both linear and controlled, a common displacement vector was established and force data were interpolated to create the independent variable utilized for the BioRank (BR) calculation (Table III). Both the right fourth and sixth ribs demonstrated overall BR under 2.0, suggesting a biofidelic response [19].

TABLE III
BIOFIDELITY RANKS FOR GHBMC INDIVIDUAL RIBS

Condition	*Force-Displacement*
Right Rib 4	1.24
Right Rib 6	0.83

Stiffness of GHBMC right fourth and sixth ribs were 3.1 and 3.0 N/mm, respectively. In comparison, the average stiffness for the same two ribs calculated from experimental rib testing were 2.5±0.8 and 4.6±1.0 N/mm, respectively. The GHBMC fourth rib displayed a stiffer response in comparison with the experimental rib data for the corresponding rib, while the sixth rib showed a softer response compared to its physical counterpart.

Fig. 9 and Fig. 10 show the effective plastic strain (EPS) contours for the cortical bone of fourth and sixth ribs respectively at peak displacement in the simulations where BPM was applied. The strain values were highest in the elements closer to the vertebral end. Ribs were instrumented with strain gages in the physical tests at 30% and 60% of rib curve length (Cv.Le), measured from the vertebral end. The peak strain values from the 30% gage location from the individual rib tests are tabulated along with the corresponding GHBMC rib strains in Table IV. The cortical strain magnitudes in the experiments at the high strain location seen in the simulations were in general lower than those predicted by GHBMC. It must be noted that the peak strain during physical rib testing occurred at the 60% location, corresponding to where fractures often occurred. The simulations with impactor loading resulted in a fracture as the elements were deleted upon reaching the defined failure EPS of 1.8% of the cortical bone. Fig. 11 shows the EPS contours for the cortical bone of fourth and sixth ribs along with the fracture location in the simulations where impactor loading was applied.

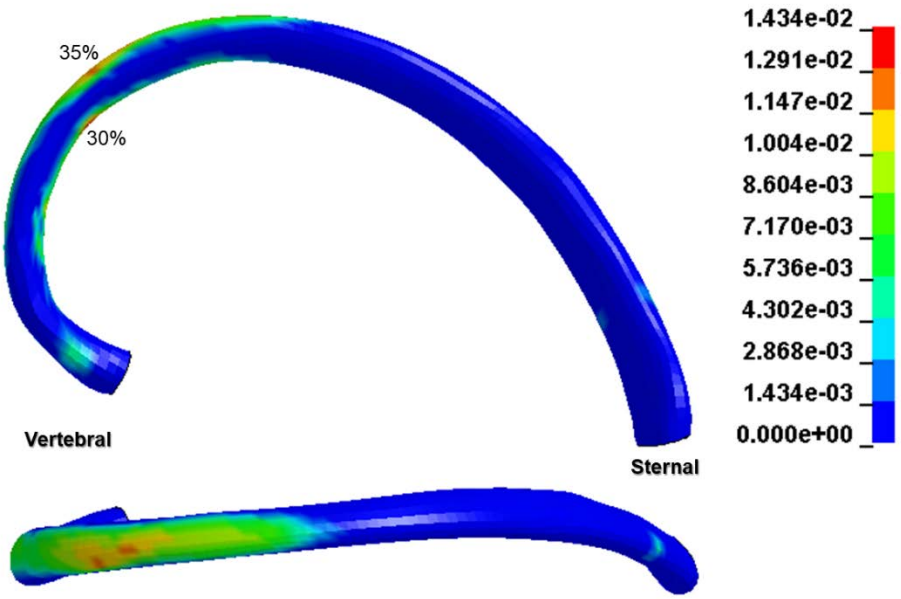

Fig. 9. Maximum effective plastic strain distribution of rib 4 under BPM loading

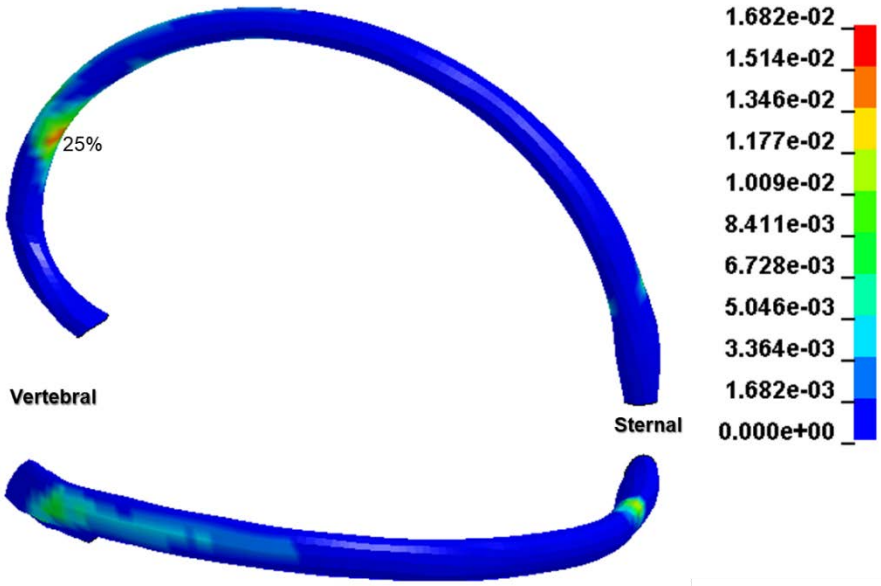

Fig. 10. Maximum effective plastic strain distribution of rib 6 under BPM loading

TABLE IV
INDIVIDUAL RIB TESTS AND SIMULATION PEAK RIB STRAINS @ 30% CV.LE; P – PLEURAL, C- CUTANEOUS

Rib #	*PMHS Avg. ± 1 St. Dev*	*GHBMC_BPM*
4	0.0099 ± 0.0053 (P)	0.0143
6	0.0121 ± 0.0061 (C)	0.0168

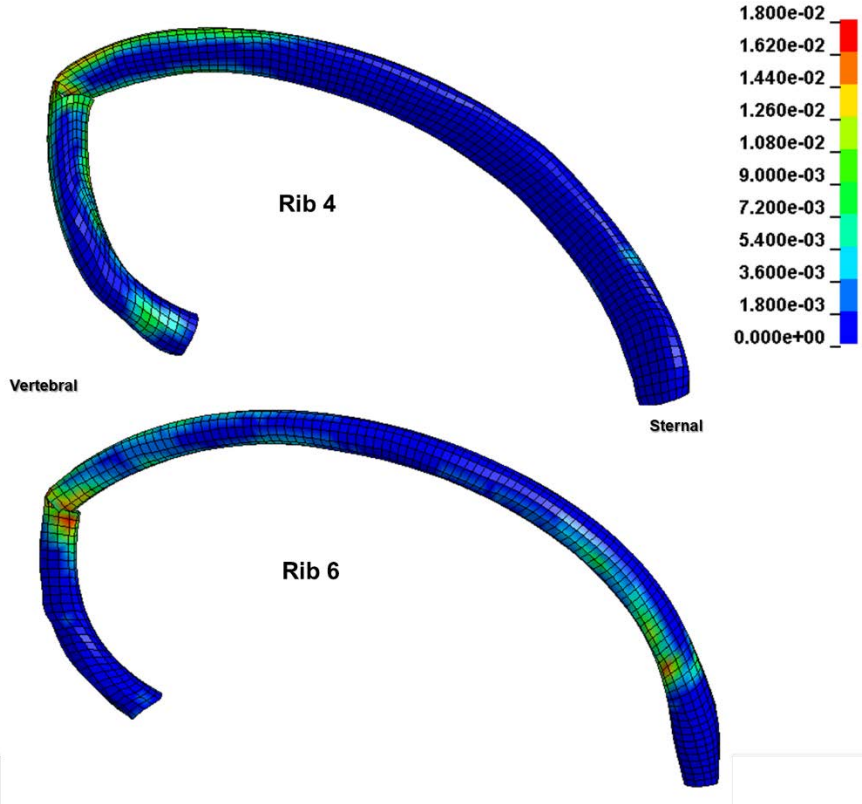

Fig. 11. Maximum effective plastic strain distribution of ribs 4 and 6 under impactor loading

IV. DISCUSSION

The objective of this study was to evaluate the biofidelity of the GHBMC thorax subjected to a dynamic loading scenario similar to experiments conducted by [13] for different tissue states, confirming whether it is appropriate to use the model to help quantify the contributions of superficial tissue, viscera, and the rib cage to thoracic response when subjected to anterior hub loading.

The GHBMC thorax was subjected to dynamic loading under four different tissue states. The responses were evaluated qualitatively and quantitatively by the development of corridors from the PMHS tests detailed in [13] and comparing the simulation results to the experiments using the Biofidelity Ranking System (BRS) [15]. For the purposes of a model evaluation, it is important that the simulation have a consistent input as the experiment. The pneumatically-driven impactor used during experimental testing provided an initial impact velocity of 3 m/s, but decelerated at a rate that was dependent on the resistance of the individual PMHS thorax. To simulate this, an initial velocity of 3 m/s was applied to a 23 kg impactor at the point of contact, but allowed to decelerate due to the response of the GHBMC thorax.

Overall, the GHBMC model showed good agreement with the experimental data in three of four states quantitatively with Biorank scores between 1.5 and 1.6. Based on the biofidelity evaluation of ATDs in [13], the GHBMC had a more human-like response than the Hybrid III 50th and THOR-50M compared to these 50th percentile subjects. The overall stiffness was also within the range observed in the PMHS tests, with the exception of the denuded case.

The GHBMC in the intact and upper limbs removed condition showed a softer initial response compared to the PMHS, suggesting a lack of mass recruitment upon impact. This may be attributed to some compliance observed in the skin and musculature outside the rib cage, both at the contact surfaces of the impactor and back plate. Increasing the stiffness of these structures could potentially resolve this variation, which will be investigated in a follow up study.

The GHBMC with the denuded condition had marginal biofidelity with a score of 2.4, and much of it may be attributed to the deviation of force in the middle 10% of chest compression compared to the PMHS. The force starts to rapidly rise after five percent chest compression suggesting a sudden mass accumulation in the thoracic cavity. This contributed to a greater stiffness value compared to the GHBMC intact condition and also compared to the PMHS tests with a denuded thorax. Upon a closer look at the simulation with a denuded thorax, it appears as if the impactor motion begins with sternum contact, which quickly changes to contact with the costal cartilage as it disengages from the sternum (Fig. 12). This phenomenon is observed at the simulation time of 5 ms, which coincides with the 5% chest compression where the contact force holds steady followed by a rapid increase. A similar sequence is noticed when the GHBMC thorax is eviscerated; however, due to the lack of organs behind the rib cage, there is no mass accumulation in the cavity leading to a softer response.

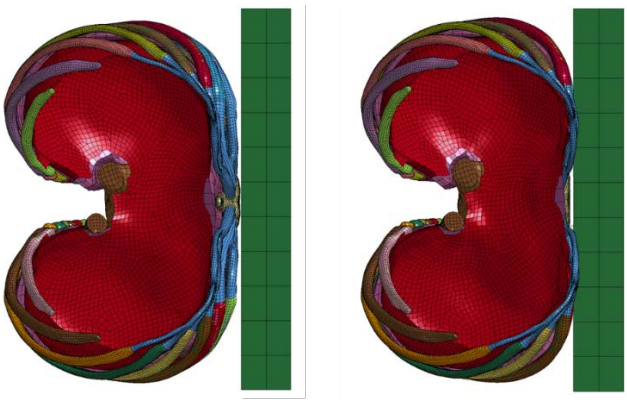

Fig. 12. Top-down view of impactor contact with the GHBMC thorax in the denuded condition. The impactor is in contact with the sternum at the beginning of the simulation (left) then disengages from the sternum and is in contact with the costal cartilage of ribs four through six at 5% chest compression.

The acceptable biofidelity score in the GHBMC with intact thorax suggests that there is good coupling between the skin, musculature, rib cage and thoracic organs. However, the marginal score when the thorax is denuded could be attributed to the material properties or the overall geometry of individual organs within the thorax. The GHBMC was made with the goal of simulating full PMHS response, and it is therefore anticipated that it should have decent biofidelity for the intact condition. If biofidelity of each sub-system such as the ribs, organs and skin are improved, the overall response of the system should improve.

Although the biofidelity scores were acceptable, the force-compression response did not completely fall within the corridor based on PMHS tests. Some of the deviation from the corridor may be attributed to the initial spinal posture. In the PMHS tests, the specimens were supported using a head-halter attached to a frame superiorly that allowed for seating the specimen upright while extending the spine. In the simulations, importance was placed in matching the sternal and rib angles, although there was a difference in the thoracic spine curvature. In order to have more comparable spinal postures between the PMHS and GHBMC, a pre-simulation in the FE study would be required, which was not included as a part of this study. A trial pre-simulation to change the spinal posture to match with the experiment resulted in change of the sternum and rib angles, leading to a mis-alignment of the impactor face with the sternum, and so was not included.

The force response in the eviscerated condition exhibits sinusoidal oscillation behavior early on in the simulation, as the force drops close to zero. This behavior is due to frictional characteristics applied between the impactor and the bony ribcage, leading to a loss of contact between the two surfaces. Additionally, the absence of damping between the contact surfaces may have led to vibration of structures and harmonic excitations. This phenomenon will be studied further using frequency response analyses.

In the individual rib simulations, the force-displacement values were comparable to the responses from rib tests in [13]. However, the GHBMC fourth rib displayed a stiffer response in comparison with the PMHS data for the corresponding rib, while the sixth rib response was on the softer end of the PMHS spectrum. The peak strain values were higher than the average strain values seen in the experiments. The high strain distribution and fracture locations predicted by GHBMC ribs were closer to the vertebral end, whereas in the experiments, fractures occurred near the sternal end. This behavior was consistent with what was observed by [17] in their simulations with reconstructed ribs, where the predicted fractures were different from those observed experimentally where the fractures occurred at anterior regions of the ribs.

The inaccuracy of fracture prediction may be attributed to several factors including but not limited to material properties, geometry, failure strain, cortical thickness distribution and rate of loading. The GHBMC uses variable thickness shell elements for cortical bone of ribs, with thicknesses ranging from 0.2 to 2.7 mm. These values are based on a study by [20], developed using elderly Asian males, and may not be representative of 50^{th} percentile American males. However, the cortical part of the rib is thinner anteriorly and gets thicker as it moves closer to the vertebral end. So, the thickness distribution may not explain the reason for differences in fracture locations.

The rib is defined by an elastic-plastic material property in the GHBMC, with plastic failure defined at 1.8% and 13% plastic strain for the cortical and trabecular bones, respectively. These values are representative of a 50 year old occupant [21]. Even if the average plastic strain values from the individual rib tests of [13] was used in the rib simulation of the current study, the high strain concentration would still be in the same location as observed with default values. However, the effect of change in yield stress and Young's Modulus based on the experiments requires investigation.

The cortical bone of the GHBMC rib is modeled using Belytschko-Tsay fully integrated thin-shell formulation where bending stiffness is negligible. Such an element type may not be able to provide accurate results in simulations where bending due to shear locking effects are predominant [22]. Anterior-posterior loading to the thorax or ribs would introduce such a phenomenon and response prediction could potentially benefit from investigating enhanced formulation and hourglass control techniques. The current shell formulation uses three

integration points through the thickness, but [23] suggests choosing four or five integration points for non-linear materials and ignoring the difference in stress between the surface and the outermost integration point.

While the GHBMC is meant to represent a 50th percentile male anthropometry, the geometric data were obtained using a single specimen of age 26; therefore, the model does not capture morphological variation in the rib cage or individual ribs, such as density, porosity and geometry. Given that the average age of subjects tested by [13] and simulated here was 66, the outcomes observed in these simulations are not necessarily representative of the geometry of a 26 year old from which the model was developed. Given the geometric variation between the model and PMHS in addition to the amount of human variation that can be found within the demographics bins currently utilized by the biomechanics community, development of subject specific models to investigate responses in detail is warranted. In [24], the ribcage geometry, cortical thickness, and material properties of the GHBMC model were modified to represent that of a 65 year-old, and a similar approach could perhaps yield better responses of both overall thorax and individual rib FE models. The PMHS study by [13] collected computer tomography (CT) scans of each subject tested and documented in detail the tissue properties such as sub-cutaneous tissue thickness and organ mass and dimensions. Using this information, the GHBMC model can be modified in terms of both geometry and material properties to better represent the corresponding subject and the relative contributions of these variations may be assessed.

The overall goal of this study is to provide updated and accurate biomechanical targets for ATDs and HBMs of various demographics. The essence of this preliminary simulation work is that it can be used in tandem with the findings from physical experiments to identify the relationship between individual rib response and overall thoracic response. Once such a relationship is established, the FE ribs from the GHBMC or any other HBM can be morphed to represent those demographics for which there is limited response data, such as the 5th percentile female or a child. Since whole-body PMHS data of these demographics are very limited, the individual rib test data that are more readily available can eventually be used to evaluate rib models that are modified to the geometry of a target population in a manner similar to this study.

Overall, using the GHBMC model to assess thoracic response in a hierarchical manner appears to be an effective approach based on the biofidelity scores and warrants furthering the study to subject-specific geometry and material properties. Such a model would allow the investigation of contributions of structures such as the intercostal muscles, costal cartilage and costovertebral ligaments to the overall thoracic response, which are harder to evaluate in an experimental setup. Additionally, given the individual rib strains were fairly similar to the experiments, structural properties of the rib may be further refined to accurately predict if a fracture occurs and where on the rib it occurs.

In summary, the study provided overall GHBMC thorax and individual rib responses in comparison with the PMHS experimental outcomes presented in [13]. The data presented in this study can be used to potentially guide material and structural changes to improve GHBMC biofidelity. Additionally, this study complements the previous PMHS study by providing information about contributions of superficial tissue, viscera, and the rib cage on the thoracic response. Future parametric exploration will provide information on appropriate mass allotments for individual organs along with material and structural properties of muscle, skin and rib parts to improve the model responses for more accurate injury prediction.

V. CONCLUSIONS

This study investigated the response of the GHBMC M50-O thorax in four tissue states, subjected to impactor loading. Biofidelity of the GHBMC thorax response in each tissue state was quantified using the NHTSA Biofidelity Ranking System (BioRank). Finally, individual fourth and sixth ribs from the GHBMC were extracted and modeled to compare with experimental rib data. The outcomes are as follows:

- The GHBMC thorax exhibited acceptable biofidelity scores (BioRank<2.0) indicating a response close to the response from a PMHS study in three of four conditions including intact, upper limbs removed and eviscerated.

- The overall stiffness was within the range observed in the PMHS tests, except in the denuded case, where it is hypothesized that the coupling characteristics present in the GHBMC thorax don't adequately reflect those same characteristics in the human thorax.
- Individual rib simulations showed similar force, displacement and stiffness responses as the experiments, however the strain values and fracture locations were not in agreement with the physical testing.

Acknowledgement

This research was supported by the National Highway Traffic Safety Administration (NHTSA), USA. Views contained within this manuscript are those of the authors and do not represent those of NHTSA.

VI. REFERENCES

[1] Arajarvi, E., and Santavirta, S. (1989) Chest Injuries Sustained in Severe Traffic Accidents by Seatbelt Wearers. Journal of Trauma 29: 37–41.

[2] Crandall, J. R., Bass, C. R., Pikey, W. D., Miller, H. J., Sikorski, J., and Wilkins, M. (1996) Thoracic Response and Injury with Belt, Driver Side Airbag, and Force Limited Belt Restraint Systems. International Journal of Crashworthiness 2(1): 119–132.

[3] Crandall, J. R., Kent, R. W., Patrie, J., Fertile, J., and Martin, P. (2000) Rib Fracture Patterns and Radiologic Detection: A Restraint-Cased Comparison. Annals of Advances in Automotive Medicine 44(1989): 235–259.Reed Allan P., et al., Clinical Cases in Anesthesia, Elsevier Health Sciences, Dec 2, 2013

[4] Lee, E. L., Craig, M., and Scarboro, M. (2015) Real-World Rib Fracture Patterns in Frontal Crashes in Different Restraint Conditions. Traffic Injury Prevention 16: S115–S123.

[5] Kimpara H, Lee JB, Yang KH, King AI, Iwamoto M, Watanabe I, Miki K. Development of a Three-Dimensional Finite Element Chest Model for the 5(th) Percentile Female. Stapp Car Crash J. 2005 Nov;49:251-69.

[6] Zhao, J., Narwani, G. (2005). Development of a human body finite element model for restraint system R&D applications. In: The 19th International Technical Conference on the Enhanced Safety of Vehicles (ESV), Washington, DC. Paper no. 05-0399.

[7] Song E, Trosseille X, Baudrit P. Evaluation of thoracic deflection as an injury criterion for side impact using a finite elements thorax model. Stapp Car Crash J. 2009 Nov;53:155-91.

[8] Ito, O., Dokko, Y., and Ohashi, K., "Development of Adult and Elderly FE Thorax Skeletal Models," SAE Technical Paper 2009-01-0381, 2009.

[9] Gayzik FS, Moreno DP, Vavalle NA, Rhyne AC, Stitzel JD. (2011) Development of the Global Human Body Models Consortium mid-sized male full body model. Injury Biomechanics Research Workshop, 2011.

[10] Kent R, Lee SH, Darvish K, Wang S, Poster CS, Lange AW, Brede C, Lange D, Matsuoka F. Structural and material changes in the aging thorax and their role in crash protection for older occupants. Stapp Car Crash J. 2005 Nov;49:231-49.

[11] Kindig MW, Lau AG, Forman JL, Kent RW. Structural response of cadaveric ribcages under a localized loading: stiffness and kinematic trends. Stapp Car Crash J. 2010 Nov;54:337-80.

[12] Poulard D, Kent RW, Kindig M, Li Z, Subit D. Thoracic response targets for a computational model: a hierarchical approach to assess the biofidelity of a 50th-percentile occupant male finite element model. J Mech Behav Biomed Mater. 2015 May;45:45-64.

[13] Murach MM, Kang YS, Bolte JH 4th, Stark D, Ramachandra R, Agnew AM, Moorhouse K, Stammen J. Quantification of Skeletal and Soft Tissue Contributions to Thoracic Response in a Dynamic Frontal Loading Scenario. Stapp Car Crash J. 2018 Nov;62:193-269.

[14] SAE, 2007. Instrumentation for impact test, Part 1: Electronic instrumentation, SAE J211/1, Society of Automotive Engineers

[15] Rhule, H, et al., A methodology for generating objective targets for quantitatively assessing the biofidelity of crash test dummies. International Technical Conference on the Enhanced Safety of Vehicles (ESV), 2009

[16]Agnew AM, Schafman M, Moorhouse K, White SE, Kang YS. The effect of age on the structural properties of human ribs. J Mech Behav Biomed Mater. 2015 Jan;41:302-14.
[17]Schafman, M. A., Kang, Y. S., Moorhouse, K., White, S. E., Bolte IV, J. H., and Agnew, A. M. (2016) Age and sex alone are insufficient to predict human rib structural response to dynamic A-P loading. Journal of Biomechanics 49(14): 3516–3522.
[18]Li Z, Kindig MW, Kerrigan JR, Untaroiu CD, Subit D, Crandall JR, Kent RW. Rib fractures under anterior-posterior dynamic loads: experimental and finite-elementstudy. J Biomech. 2010 Jan 19;43(2):228-34. doi: 10.1016/j.jbiomech.2009.08.040.
[19]Rhule, H.H., Maltese, M.R., Donnelly, B.R., Eppinger, R.H., Brunner, J.K., and Bolte, J.H.IV. (2002) Development of a New Biofidelity Ranking System for Anthropomorphic Test Devices. Stapp Car Crash Journal 46: 477-512.
[20]Choi, Y.C., Lee, I.,Thorax FE Model for Older Population, Japanese Society of Mechanical Engineers, Fukuoka (2009).
[21]Golman AJ, Danelson KA, Miller LE, Stitzel JD. Injury prediction in a side impact crash using human body model simulation. Accid Anal Prev. 2014.
[22]LS-DYNA Theory Manual, LSTC.
[23]Chapelle, D., Bathe, K.j., The Finite Element Analysis of Shells—Fundamentals, Springer-Verlag, Berlin Heidelberg New York, 2003.
[24]Schoell SL, Weaver AA, Vavalle NA, Stitzel JD. Age- and sex-specific thorax finite element model development and simulation. Traffic Inj Prev. 2015;16 Suppl 1:S57-65.

VII. APPENDIX

TABLE A1
SUBJECT DEMOGRAPHICS

	PMHS 02	*PMHS 03*	*PMHS 04*	*PMHS 05*	*PMHS 06*	*PMHS Avg. ± 1 St. Dev.*	*GHBMC M50-O*
Sex	M	M	M	M	M	N/A	M
Age (years)	73	62	55	70	59	66 ± 8	26
Stature (cm)	170	173	183	191	180	180 ± 7	175
Mass (kg)	62	84	75	79	65	72 ± 8	78
[1]BMI (kg/cm^2)	21.5	28.3	22.4	21.7	20.1	22.2 ± 2.9	25.7
[2]aBMD t-score (lumbar)	+0.4	+1.6	+1.1	+0.6	+2.1	+1.2 ± 0.6	NA
Chest Depth (cm)	25	26	22	25	20	23 ± 2	23
Chest Breadth (cm)	33	34	32	33	35	33 ± 2	32
Chest Circumference (cm)	90	108	95	105	92	97 ± 7	100
[3]Thoracic Index	0.76	0.65	0.75	0.64	0.57	0.70 ± 0.10	0.72
Sternal Height (cm)	18.7	21.1	21.5	18.5	19.2	19.7 ± 1.2	14.4
Sternal Width (cm)	4.0	3.7	4.1	5.3	3.7	4.0 ± 0.6	4.2

[1]BMI = BODY MASS INDEX (MASS/STATURE2),
[2]aBMD = AREAL BONE MINERAL DENSITY AS MEASURED BY DUAL-ENERGY X-RAY ABSORPTIOMETRY (DXA),
[3]THORACIC INDEX = CHEST DEPTH/CHEST BREADTH

TABLE A2
ANTERIOR- POSTERIOR SEATED CHEST DEPTH

Subject	*Intact (mm)*	*Intact - UL (mm)*	*Denuded (mm)*	*Eviscerated (mm)*
PMHS 02	230	230	220	225
PMHS 03	250	250	225	235
PMHS 04	205	220	200	210
PMHS 05	225	235	215	225
PMHS 06	200	200	200	200
Average	*222*	*227*	*212*	*219*
St. Dev	*18.1*	*16.6*	*10.3*	*12.4*
GHBMC M50-O	227	227	186	186

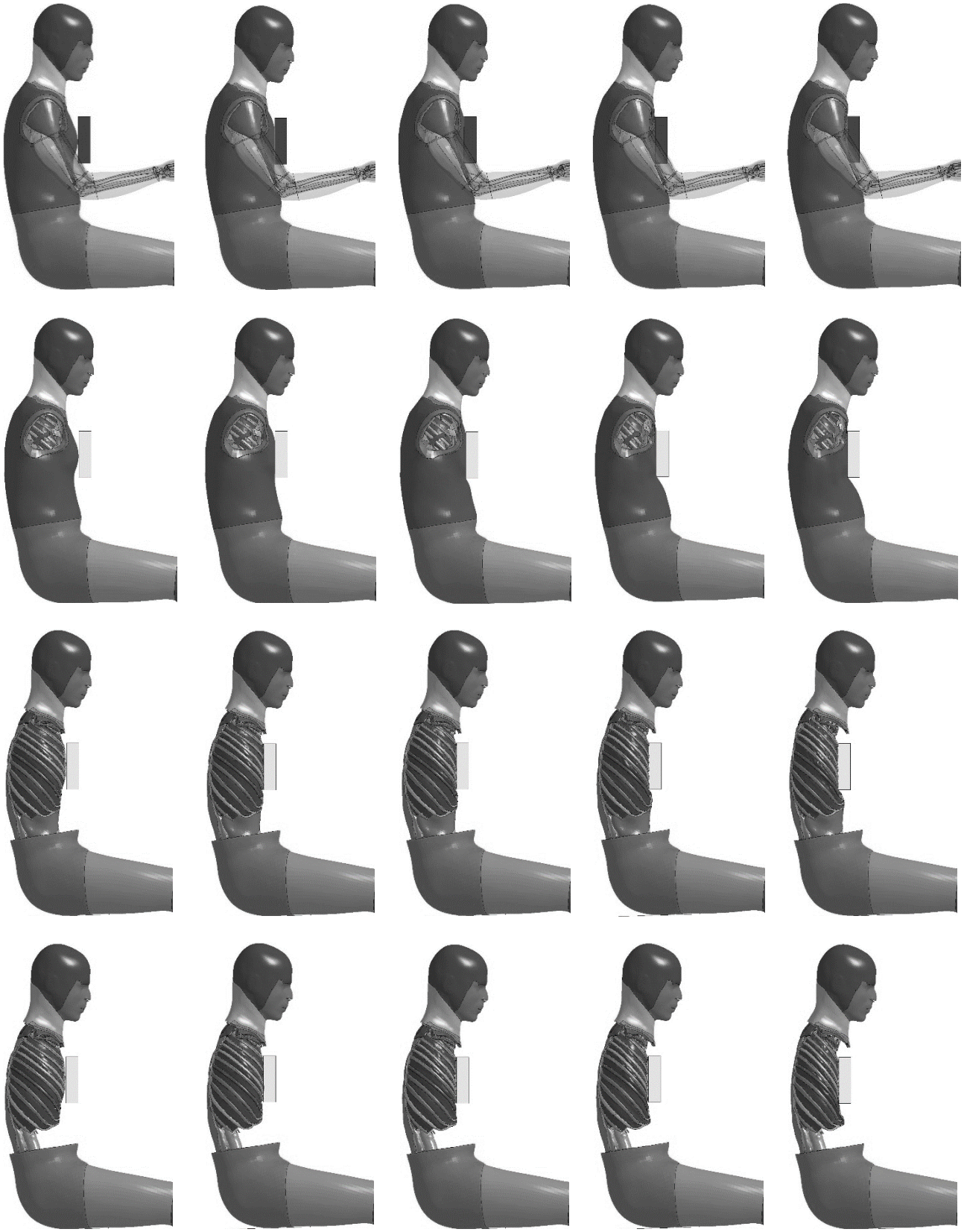

FIG. A1. SNAPSHOTS FROM THORACIC HIERARCHY SIMULATIONS AT 0, 5, 10, 15 AND 20% COMPRESSION
[TOP TO BOTTOM: INTACT, UPPER LIMBS REMOVED, DENUDED, EVISCERATED]